Tracking Breather Dynamics in Irregular Sea State Conditions

Amin Chabchoub*
Department of Mechanical Engineering, Aalto University, 02150 Espoo, Finland
and Department of Ocean Technology Policy and Environment, Graduate School of Frontier Sciences, The University of Tokyo, Kashiwa, Chiba 277-8563, Japan
(Received 20 April 2016; published 28 September 2016)

Breather solutions of the nonlinear Schrödinger equation (NLSE) are known to be considered as backbone models for extreme events in the ocean as well as in Kerr media. These exact deterministic rogue wave (RW) prototypes on a regular background describe a wide range of modulation instability configurations. Alternatively, oceanic or electromagnetic wave fields can be of chaotic nature and it is known that RWs may develop in such conditions as well. We report an experimental study confirming that extreme localizations in an irregular oceanic Joint North Sea Wave Project wave field can be tracked back to originate from exact NLSE breather solutions, such as the Peregrine breather. Numerical NLSE as well as modified NLSE simulations are both in good agreement with laboratory experiments and highlight the significance of universal weakly nonlinear evolution equations in the emergence as well as prediction of extreme events in nonlinear dispersive media.

DOI: 10.1103/PhysRevLett.117.144103

Extreme ocean waves, also referred to as freak or rogue waves (RWs), are known to appear without warning and have a disastrous impact as a consequence of the substantially large wave heights they can reach [1,2]. Studies on RWs have recently attracted scientific interest due to the interdisciplinary nature of the modulation instability (MI) of weakly nonlinear waves [3–5] as well as for the sake of accurate modeling and prediction of these mysterious extremes [6–9]. Indeed, exact solutions of the nonlinear Schrödinger equation (NLSE) provide advanced backbone models that can be used to describe the dynamics of RWs in time and space, providing, therefore, deterministic numerical and laboratory prototypes to reveal novel insights of MI [10]. Within the vast range of pulsating NLSE solutions on a finite background, there is one prominent candidate that is known to have similar physical properties as ocean RWs, namely, the doubly-localized Peregrine breather (PB) [11,12]. Despite the fact that it is theoretically assumed that the modulation period of the PB is infinite, laboratory observations confirmed that a finite number of waves in the background is sufficient to initiate its dynamics in nonlinear dispersive media [13,14]. These observations also proved that extreme localizations can be indeed discussed by means of the NLSE, despite violation of the theoretical assumption of the wave field to be and to remain narrow banded.

Based on this latest progress, it is reasonable to study the dynamics of breathers, assuming irregularity of the underlying wave field in order to quantify limitations of the approach and to enlarge the scope of possible applications such as in oceanography. In fact, the motion of ocean waves can be indeed narrow banded, such as in the case of swell. However, when winds, currents, and wave breaking are at play, the wave field may experience strong irregularities, a state that is supposed to limit applicability of the NLSE. On the other hand, recent laboratory experiments revealed, for instance, the persistence of the PB in the presence of a strong wind [15] and therefore its physical robustness to perturbations. To the best of our knowledge, the emergence of a RW in an irregular random wave field has never been tracked back to start from NLSE breather dynamics in a laboratory environment.

Here, we report an experimental study confirming the possibility for exact breather solutions to trigger extreme events in realistic oceanic conditions. According to this, the PB has been embedded into an irregular Joint North Sea Wave Project (JONSWAP)-type wave field [16], thus, into a realistic irregular ocean configuration with random phases in order to provide initial conditions for the experiments. In this latter hybrid surface elevation, the unstable Peregrine wave packet perturbation, now cloaked in the irregular state, initiates the focusing of an extreme wave that satisfies the oceanographic definition of a RW, that is, the height of the measured extreme wave indeed exceeds twice the significant wave height of the wave record. The reported results can be regarded as complementary to the experimental studies in optics [17,18] related to the emergence of coherent structures from random background perturbation. The difference here is that the PB has been seeded and stimulated in an irregular wave field rather than observed to spontaneously emerge from a noisy background. The experimental measurements are compared with NLSE and modified NLSE (MNLSE) predictions that show good agreement. This certifies the possible life span of NLSE models in broad-banded processes, a fact that may be valuable in the prediction of extreme events as well as in extending the applicability range of deterministic localized structures in optics and ocean engineering.

The unidirectional evolution of water wave packets $\Psi(x,t)$ in deep water can be modeled by means of the time NLSE [2,19]

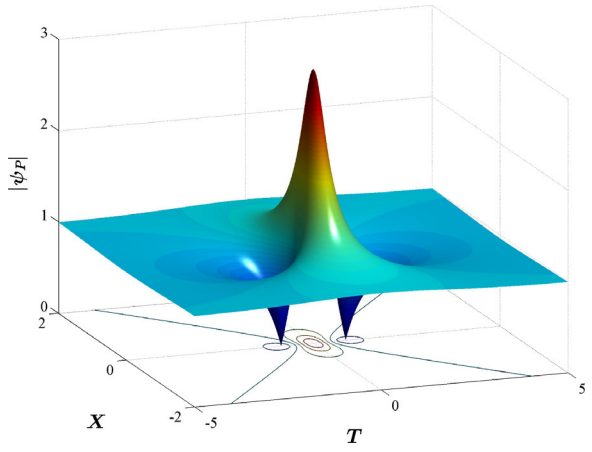

FIG. 1. Modulus of the doubly localized PB solution [Eq. (3)] as a function of scaled space and time coordinates X and T, respectively. At $X = 0 = T$ the normalized amplitude of the regular wave field is enhanced by a factor of 3.

$$i\left(\Psi_x + \frac{2k}{\omega}\Psi_t\right) - \frac{1}{g}\Psi_{tt} - k^3|\Psi|^2\Psi = 0, \tag{1}$$

where g denotes the gravitational acceleration and the wave frequency ω is connected to the wave number k through the linear dispersion relation $\omega = \sqrt{gk}$. An efficient way to model and generate a single extreme event on the water surface can be achieved by use of the PB [11]. When considering the scaled form of the time NLSE

$$i\psi_X + \psi_{TT} + 2|\psi|^2\psi = 0, \tag{2}$$

this latter solution with algebraic instability growth rate reads

$$\psi_P(X,T) = \left(-1 + \frac{4 + 16iX}{1 + 16X^2 + 4T^2}\right)\exp(2iX). \tag{3}$$

The PB solution, Eq. (3), is depicted in Fig. 1 while its physical properties are described in the caption of Fig. 1. The PB solution, Eq. (3), is the subject of intensive studies [20–22] due to its particular physical features including the fact that it describes the MI in the case of an infinite modulation period. Interestingly, this breather (or any other doubly localized solution of this kind [4,23]) does not require an infinite number of waves in order to observe its dynamics in a physical medium [24]. Based on this fact, the aim of this study is to investigate the possibility of the PB's focusing feature to persist in chaotic conditions. To achieve this, a dimensional form of the solution is embedded in an oceanic JONSWAP-type wave field, as shall be described in the following.

The experiments have been performed in a deep-water facility, see details in Ref. [25]. The dimensional amplitude of the carrier has been set to be $a = 0.75$ cm, while the wave peak frequency is $f_p = 1.70$ Hz. Thus, the steepness is $ak = 0.08$. Considering the expression of the water surface elevation to first-order of approximation being

$$\eta(x,t) = \mathrm{Re}(\Psi(x,t)\exp[i(kx - \omega t)]), \tag{4}$$

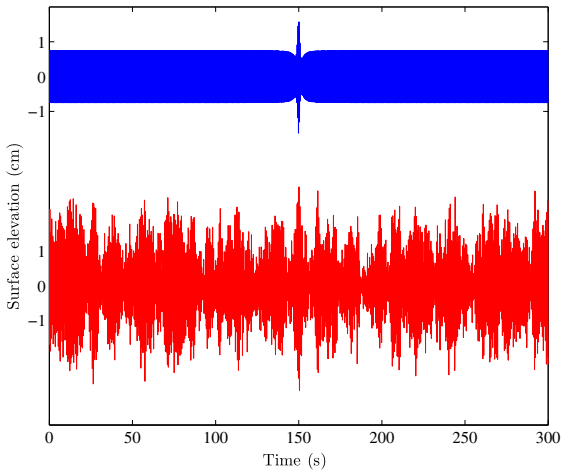

FIG. 2. Upper panel: The Peregrine water surface displacement for $ak = 0.08$ and $a = 0.75$ cm, evaluated at $x = -6$ m (blue line). Lower Panel: The surface displacement of the PB surface realization, displayed in the upper panel, embedded in a JONSWAP wave field having a significant wave height of 3 cm with peak enhancement factor $\gamma = 6$ at the same frequency peak of $f_p = 1.70$ Hz (red line). This signal will then be used to generate the wave motion by the wave maker.

the temporal surface displacement of the Peregrine model $\eta_P(t)$ is determined in the expectation to observe the theoretical maximal breather compression 6 m from the wave generator, i.e., $\eta_P(t) = \eta_P(x = -6, t)$, see upper panel of Fig. 2. In the next step, $\eta_P(t)$ was embedded in a chaotic wave field. Generally, one possible way to generate realistic oceanic sea states, is for the energy of the irregular wave field to satisfy a JONSWAP spectrum [26]

$$S(f) = \frac{\alpha}{f^5}\exp\left[-\frac{5}{4}\left(\frac{f_p}{f}\right)^4\right]\gamma^{\exp[-(f-f_p)^2/(2\sigma^2 f_p^2)]}. \tag{5}$$

We set the frequency peak at $f_p = 1.70$ Hz, the significant wave height of the wave field, defined as 4 times the standard deviation of the wave field [1], to be $H_s = 3$ cm, and the peak enhancement factor $\gamma = 6$. Furthermore, $\sigma = 0.09$ if $f > f_p$ and $\sigma = 0.07$ if $f \le f_p$. Note that the JONSWAP spectrum is just a peaked-enhanced extension of the Pierson-Moskowitz spectrum [26]. A JONSWAP surface displacement realization with random phases $\varphi_n \in]0, 2\pi[$ is then determined by [27]

$$\eta_{\mathrm{JONSWAP}}(0,t) = \sum_{i=1}^{N}\sqrt{2S(f_n)\Delta f_n}\cos(2\pi f_n t - \varphi_n). \tag{6}$$

The Peregrine surface elevation $\eta_P(t)$ is now added to a JONSWAP realization with random phases $\eta_R(t)$, as described above and modeled in Fourier space accordingly, so that the new constructed hybrid surface elevation

$$\eta_{\mathrm{hybrid}}(t) = \eta_P(t) + \eta_R(t) \tag{7}$$

has the energy peak of $\eta_P(t)$. The hybrid time series Eq. (7) is therefore a JONSWAP realization, for parameters as mentioned above, with an embedded Peregrine-type wave packet. Therefore, typical Peregrine model characteristics

are embedded in the hybrid surface elevation [Eq. (7)] as well. The latter is shown in the lower panel of Fig. 2 and is now chosen as a boundary condition to drive the wave maker. We point out that the unstable Peregrine envelope perturbation is now cloaked in the JONSWAP wave train, which reveals several wave modulations that are similar in wave height as the Peregrine-type wave packet. Note that MI in JONSWAP random sea states has been discussed in a general context, for instance, theoretically, within the framework of the NLSE and the inverse scattering transform (IST) in Refs. [2,28], while numerically in Refs. [27,29,30] and experimentally in Ref. [31]. The specific unstable wave packet considered here and located around 150 s in the JONSWAP wave train is characterized by PB features. The focusing of the latter during its evolution proves that breather-type waves may exist and persist locally, even in the case of an irregular or strongly perturbed background. This would also emphasize the importance of integrable systems in the possible detection of unstable and local wave packets in the ocean.

The evolution of the generated wave field is measured equidistantly at nine positions along the wave flume. The last wave gauge is placed 9 m from the wave maker, that is still at 3 m distance from the beach, hence, far enough to be affected by strong wave reflections. Figure 3 depicts the propagation of the wave field with particular emphasis on the hybrid Peregrine packets, namely, in the intervals bounded by the dashed lines.

Indeed, we can clearly notice a significant focusing during the propagation of the Peregrine-type wave packet evolving in the irregular water wave configuration. The maximal wave is measured at 7 m in the experiment and highlights a wave height of 5.22 cm. This latter wave train is isolated and shown separately in Fig. 4. The time delay of the extreme localization compared to the corresponding initial small localization in Fig. 2 corresponds to the delay

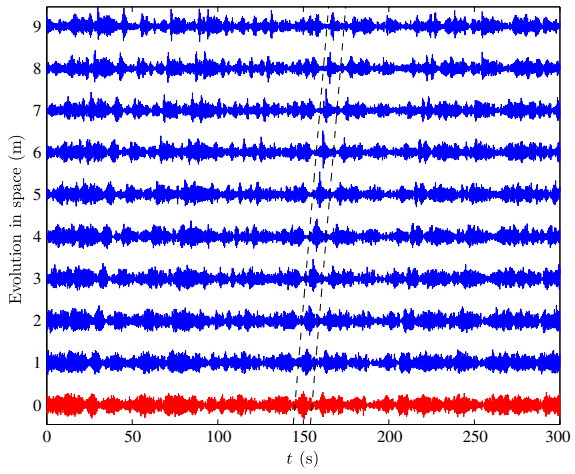

FIG. 3. Evolution of the hybrid JONSWAP-Peregrine wave field over 9 m. The bottom time series (red curve) illustrates the boundary condition applied to the wave maker, while the dashed lines limit the unstable Peregrine packet, moving with the group velocity $c_g = \omega/(2k) = 0.46\ \mathrm{m}\cdot\mathrm{s}^{-1}$.

expected for the unstable wave packet to propagate with the group velocity over 7 m. As a matter of fact, we can state that this Peregrine-type extreme wave is indeed a RW, since the abnormality index of the maximal wave, defined as being the ratio of maximal wave height and significant wave height, exceeds two [1]. Other physical features of this extreme wave are summarized in Table I.

It is emphasized that due to strong focusing of the wave, slight spilling breaking has been observed during the evolution. Nevertheless, these measurements prove that Peregrine dynamics may indeed persist in a random one-dimensional sea state with strong irregularities, allowing, therefore, the tracking of an extreme oceanic event to backbone models of integrable evolution equations. This also justifies, once again, the choice of investigating fundamental theoretical as well as physical properties of exact NLSE solutions in order to accurately predict RWs in the ocean [1,2]. We also observe the focusing of other wave packets in the JONSWAP wave train that may have their origin in modulation instability. However, none of these reach the amplitude amplification of the hybrid Peregrine wave packet. Here, the IST detection method [2,32] may be a useful technique in characterizing and identifying the instability mechanisms of these latter packets.

Next, the experimental wave evolution is compared to numerical simulations, based on NLSE and MNLSE, using the split-step method. The time MNLSE [33,34] reads

$$i\left(\Psi_x + \frac{2k}{\omega}\Psi_t\right) - \frac{1}{g}\Psi_{tt} - k^3|\Psi|^2\Psi - i\frac{k^3}{\omega}\left\{6|\Psi|^2\Psi_t + 2\Psi(|\Psi|^2)_t - 2i\Psi\mathcal{H}[(|\Psi|^2)_t]\right\} = 0, \tag{8}$$

while $\mathcal{H}$ denotes the Hilbert transform. The MNLSE is an extension of the NLSE that improves approximation of

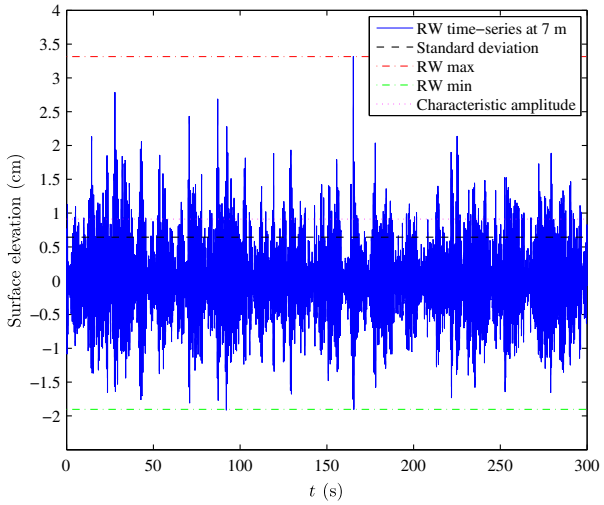

FIG. 4. Temporal wave displacement of the maximal Peregrine-type RW, measured 7 m from the wave maker. The horizontal lines are described in the figure's legend.

TABLE I. Characteristic properties of the maximal wave in the 300 s wave train, measured 7 m from the wave generator.

Standard deviation	Characteristic amplitude	Significant wave height	Maximal height	Abnormality index
$\sigma = 0.64$ cm	$a_{\text{char}} = 0.90$ cm	$H_s = 2.56$ cm	$H_{\max} = 5.22$ cm	$AI = 2.04$

dispersion and that takes into account the mean flow of the wave field. The surface measurement, restricted to 120 s and aligned with respect to the group velocity c_g, as well as both simulation results, are illustrated in Fig. 5. Both simulation results are in qualitatively good agreement with the laboratory experiments. We recall that neither the NLSE nor the MNLSE can model the breaking of the wave field since at this stage of approximation the wave field is assumed to be irrotational, among other limitations. In fact, both evolution equations prove to be very accurate in predicting the extreme event, occurring roughly at the expected distance from the wave generator, while surrounding modulated wave packets remain quasi-stable during their evolution. Furthermore, it is interesting to notice that the maximal wave amplification in the MNLSE prediction is retarded while being slightly lower compared to the NLSE simulations, as expected [35]. Even though being generally less accurate than the MNLSE when the wave process becomes broad banded [36–38], the NLSE simulations surprisingly provide a better estimate to the start of growth and decay of wave envelope compression in the experiment. Generally, the occurrence of wave breaking prevents the flawless computation of the field envelope. The complex breaking effects can be captured by performing computationally extensive and advanced numerical simulations solving the Navier-Stokes equations [39,40]. Nonetheless, the simulations reported in the study vindicate the significance of weakly nonlinear evolution equations in modeling the motion of ocean waves [41,42].

To conclude, we have shown that doubly localized PB dynamics may persist on an irregular background. Indeed, the constructed hybrid Peregrine-JONSWAP wave field with random phases is shown to generate a hydrodynamic extreme event at the expected temporal and spatial locality. The observed highest wave has an abnormality index that exceeds two, satisfying the definition of ocean RWs. The experimental results are effectively in good agreement with NLSE and MNLSE simulations, both are accurate in the prediction

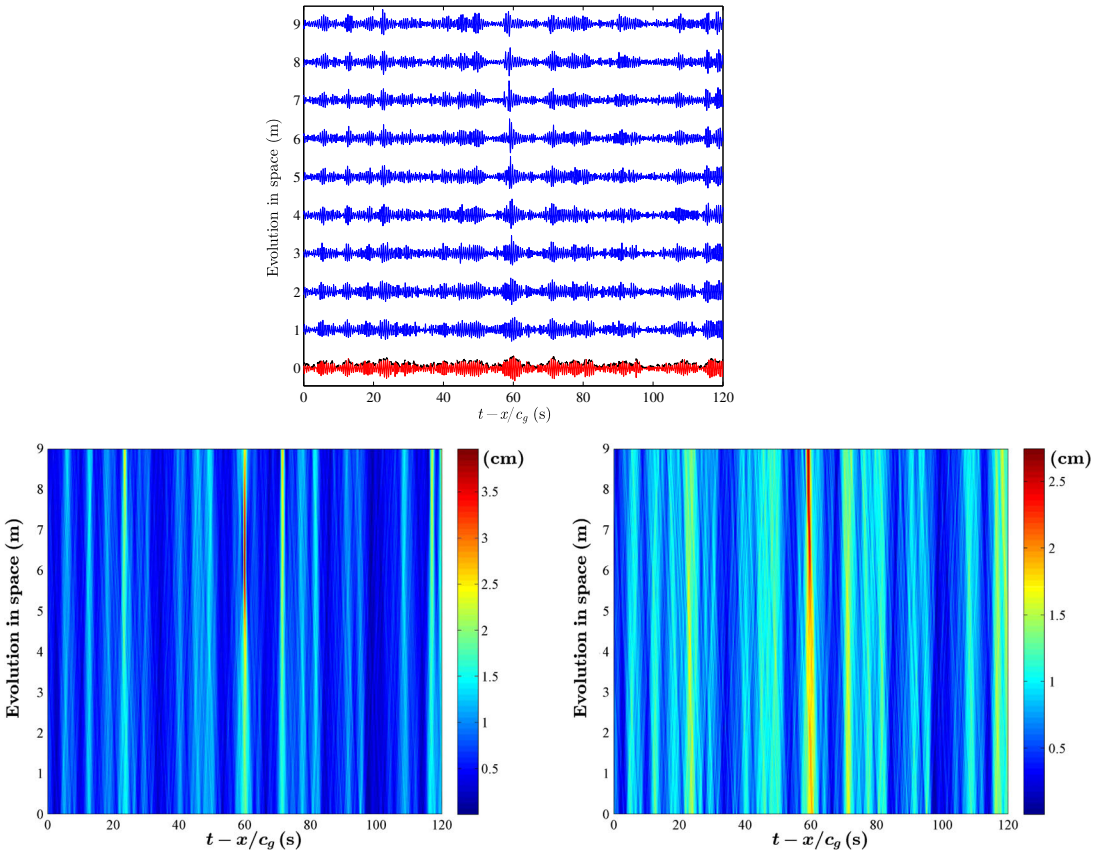

FIG. 5. Upper panel: Surface displacements aligned by the value of the group velocity c_g. The envelope of the experimental initial conditions at the wave maker's position is computed by means of the Hilbert transform and its modulus is depicted in black dashed lines. Lower left panel: NLSE simulation prediction results, starting from the computed Hilbert envelope. Lower right panel: MNLSE simulation prediction results, also starting from the same computed Hilbert envelope as for the NLSE simulations.

of the single extreme event despite constraints in the modeling that does not include viscosity, dissipation, breaking, and other limitations associated to laboratory experiments. Future work will characterize the influence of initial JONSWAP amplitudes, mode phases as well as spectral parameters α and γ, which have a significant influence when interacting with NLSE breathers in the described approach. Numerical simulations based on more accurate evolution equations, such as the higher-order spectral method [43,44], may also determine the limitations of the approach as well as reveal new insights into the problem, taking into account that the latter are much faster to perform compared to laboratory experiments. This study also discloses that characteristic breather spectral properties in the physical domain [45], as well as in the IST plane [2,32] and the distinctive energy signature of focusing localized structures [46], are indeed promising features that can be applied for the sake of accurate deterministic oceanic extreme event detection. To round the picture, the role of breather applications on realistic directional sea states is still to be discovered and needs further investigation [29,47,48]. Because of the interdisciplinary character of the approach [49], it is expected that analogous numerical and experimental studies may be motivated, for instance, in Kerr media and plasma, hence, improving the decryption of RWs as well as nonlinear localized wave packets in regular and irregular sea states.

A. C. acknowledges support from the Japan Society for the Promotion of Science (JSPS) and the Burgundy Region (PARI Photcom).

*amin.chabchoub@aalto.fi

[1] C. Kharif, E. Pelinovsky, and A. Slunyaev, *Rogue Waves in the Ocean* (Springer, New York, 2009).
[2] A. Osborne, *Nonlinear Ocean Waves & the Inverse Scattering Transform*, Vol. 97 (Academic Press, New York, 2010).
[3] T. B. Benjamin and J. Feir, J. Fluid Mech. **27**, 417 (1967).
[4] N. Akhmediev, V. M. Eleonskii, and N. E. Kulagin, Sov. Phys. JETP **62**, 894 (1985).
[5] V. E. Zakharov and A. A. Gelash, Phys. Rev. Lett. **111**, 054101 (2013).
[6] C. Kharif and E. Pelinovsky, Eur. J. Mech. B **22**, 603 (2003).
[7] M. Onorato, S. Residori, U. Bortolozzo, A. Montina, and F. T. Arecchi, Phys. Rep. **528**, 47 (2013).
[8] J. M. Dudley, F. Dias, M. Erkintalo, and G. Genty, Nat. Photonics **8**, 755 (2014).
[9] F. Baronio, M. Conforti, A. Degasperis, S. Lombardo, M. Onorato, and S. Wabnitz, Phys. Rev. Lett. **113**, 034101 (2014).
[10] N. Akhmediev and A. Ankiewicz, *Solitons: Nonlinear Pulses and Beams* (Chapman and Hall, London, 1997).
[11] D. H. Peregrine, J. Aust. Math. Soc. Series B, Appl. Math. **25**, 16 (1983).
[12] V. I. Shrira and V. V. Geogjaev, J. Eng. Math. **67**, 11 (2010).
[13] B. Kibler, J. Fatome, C. Finot, G. Millot, F. Dias, G. Genty, N. Akhmediev, and J. M. Dudley, Nat. Phys. **6**, 790 (2010).
[14] A. Chabchoub, N. P. Hoffmann, and N. Akhmediev, Phys. Rev. Lett. **106**, 204502 (2011).
[15] A. Chabchoub, N. Hoffmann, H. Branger, C. Kharif, and N. Akhmediev, Phys. Fluids **25**, 101704 (2013).
[16] A. Babanin, *Breaking and Dissipation of Ocean Surface Waves* (Cambridge University Press, Cambridge, 2011).
[17] P. Walczak, S. Randoux, and P. Suret, Phys. Rev. Lett. **114**, 143903 (2015).
[18] P. Suret, R. E. Koussaifi, A. Tikan, C. Evain, S. Randoux, C. Szwaj, and S. Bielawski, arXiv:1603.01477.
[19] V. E. Zakharov, J. Appl. Mech. Tech. Phys. **9**, 190 (1968).
[20] M. Onorato, D. Proment, G. Clauss, and M. Klein, PLoS One **8**, e54629 (2013).
[21] R. Grimshaw and A. Tovbis, Proc. R. Soc. A **469**, 20130094 (2013).
[22] A. Chabchoub and M. Fink, Phys. Rev. Lett. **112**, 124101 (2014).
[23] N. Akhmediev, A. Ankiewicz, and J. M. Soto-Crespo, Phys. Rev. E **80**, 026601 (2009).
[24] A. Chabchoub, M. Onorato, and N. Akhmediev, *Rogue and Shock Waves*, edited by M. Onorato, S. Residori, and F. Baronio, Lecture Notes in Physics (Springer, New York, 2016).
[25] B. Kibler, A. Chabchoub, A. Gelash, N. Akhmediev, and V. E. Zakharov, Phys. Rev. X **5**, 041026 (2015).
[26] G. J. Komen, L. Cavaleri, M. Donelan, K. Hasselmann, S. Hasselmann, and P. Janssen, *Dynamics and Modelling of Ocean Waves* (Cambridge University Press, Cambridge, 1996).
[27] M. Onorato, A. R. Osborne, M. Serio, and S. Bertone, Phys. Rev. Lett. **86**, 5831 (2001).
[28] A. Islas and C. Schober, Phys. Fluids **17**, 031701 (2005).
[29] S. Toenger, T. Godin, C. Billet, F. Dias, M. Erkintalo, G. Genty, and J. M. Dudley, Scientific Reports **5**, 10380 (2015).
[30] J. M. Soto-Crespo, N. Devine, and N. Akhmediev, Phys. Rev. Lett. **116**, 103901 (2016).
[31] M. Onorato, A. Osborne, M. Serio, L. Cavaleri, C. Brandini, and C. Stansberg, Eur. J. Mech. B **25**, 586 (2006).
[32] S. Randoux, P. Suret, and G. El, Scientific reports **6**, 29238 (2016).
[33] K. B. Dysthe, Proc. R. Soc. A **369**, 105 (1979).
[34] K. Trulsen and C. T. Stansberg, in *The Eleventh International Offshore and Polar Engineering Conference* (International Society of Offshore and Polar Engineers, Stavanger, 2001).
[35] A. Slunyaev, E. Pelinovsky, A. Sergeeva, A. Chabchoub, N. Hoffmann, M. Onorato, and N. Akhmediev, Phys. Rev. E **88**, 012909 (2013).
[36] K. Trulsen and K. B. Dysthe, Wave Motion **24**, 281 (1996).
[37] A. Chabchoub, N. Hoffmann, M. Onorato, G. Genty, J. M. Dudley, and N. Akhmediev, Phys. Rev. Lett. **111**, 054104 (2013).
[38] L. Shemer and L. Alperovich, Phys. Fluids **25**, 051701 (2013).
[39] A. Iafrati, A. Babanin, and M. Onorato, Phys. Rev. Lett. **110**, 184504 (2013).
[40] R. Perić, N. Hoffmann, and A. Chabchoub, Eur. J. Mech. B **49**, 71 (2015).
[41] K. Trulsen, in *Geometric Modelling, Numerical Simulation, and Optimization* (Springer, New York, 2007), pp. 191–209.
[42] A. Toffoli, T. Waseda, H. Houtani, T. Kinoshita, K. Collins, D. Proment, and M. Onorato, Phys. Rev. E **87**, 051201 (2013).

[43] G. Ducrozet, F. Bonnefoy, D. Le Touzé, and P. Ferrant, Eur. J. Mech. B **34**, 19 (2012).
[44] A. V. Slunyaev and V. I. Shrira, J. Fluid Mech. **735**, 203 (2013).
[45] N. Akhmediev, A. Ankiewicz, J. Soto-Crespo, and J. M. Dudley, Phys. Lett. A **375**, 541 (2011).
[46] W. Cousins and T. P. Sapsis, J. Fluid Mech. **790**, 368 (2016).
[47] S. Birkholz, C. Brée, A. Demircan, and G. Steinmeyer, Phys. Rev. Lett. **114**, 213901 (2015).
[48] F. Fedele, J. Brennan, S. P. De León, J. Dudley, and F. Dias, Scientific reports **6**, 27715 (2016).
[49] B. Wetzel, D. Bongiovanni, M. Kues, Y. Hu, Z. Chen, S. Trillo, J. M. Dudley, S. Wabnitz, and R. Morandotti, Phys. Rev. Lett. **117**, 073902 (2016).